S. Gopinath*, M. Sundararaj, S. Elangovan and E. Rathakrishnan

Mixing Characteristics of Elliptical and Rectangular Subsonic Jets with Swirling Co-flow

Abstract: This paper presents a computational analysis of effects of swirling co-flow and non-circular subsonic compressible inner jets on centerline velocity decay, mass entrainment and jet spreading rate. Three different exit shapes of elliptical, rectangular and circular inner jets were compared for three different co-flow conditions such as no co-flow, straight co-flow and swirling co-flow. Co-flow is issuing from a circular annular duct. Swirling co-flow is created in the co-flow duct by introducing a swirler with stationary angular vanes of 50° oblique to the jet axis. Reynolds number of inner jet is calculated based on its equivalent diameter as 200342. It is found that the swirling co-flow has strong influence on the boundary condition of inner jet and alters the major features of the jet such as jet potential core length, centerline velocity decay rate and jet spread rate. Streamwise corner vortices of different jet conditions have been captured using velocity vector plot to show the effect of swirling co-flow on the jet flow field. Swirling co-flow with elliptical inner jet exhibits higher velocity decay rate and jet spreading rate than the equivalent area circular and rectangular jet.

Keywords: rectangular jet, elliptical jet, subsonic free jet, co-flow, swirling co-flow

PACS® (2010). 47.27.wg, 47.32.Ef, 47.15.Ef

DOI 10.1515/tjj-2014-0015
Received June 10, 2014; accepted June 18, 2014.

1 Introduction

Jet issuing from a nozzle has been implemented in gas turbine combustor, jet exhaust, cooling systems, gas welding and various other industrial applications. Understanding of the mixing characteristics of jets helps us to improve the efficiency and effectiveness of such engineering applications. This study is aimed at investigation of the effect of swirling co-flow on the mixing characteristics of non-circular inner jet.

Phenomenon of jet mixing has been a topic of research for many years and presented in numerous papers. Hussein et al. [1] investigated a turbulent jet issued from a circular jet exhaust into a large room. He presented a detail results of jet flow characteristics acquired by using flying hot-wire and burst mode LDV technique. In order to study the influence of Reynolds number on self-similarity of jets, Bogey and Bailly [3] conducted large-eddy simulation for circular jets with three different Reynolds numbers (1800, 3600 and 11000). He stated that the effects of Reynolds number were found to be weak on the turbulent kinetic energy and velocity moments across the self-similar jet flow. Low Reynolds number jet flow attains self-similarity more rapidly than the high Reynolds number jet flow. Gutmark and Grinstein [2] studied the enhancement of combustor performance by small and large scale mixing of jets issued from circular and non-circular exits. Incorporation of non-circular exit geometry will enhance fuel mixing efficiency by reducing mixing instabilities and undesired emission of noise. Non-circular jet flow involves fine scale turbulence augmentations, interaction and evolution of corner vortices. He also concluded that the jet flow field was strongly influenced by the exit geometry. Miller et al. [6] presented numerical simulation of three dimensional non-circular nozzles of identical equivalent diameters. He studied elliptic, triangle and rectangular jets with different aspect ratio (AR = 1 and AR = 2) and concluded that all non-circular nozzles were efficient mixers than the circular nozzles. Axis switching and streamwise vortex structure were also presented in detail. Srinivasan and Rathakrishnan [10] conducted experiments to study the effect of aspect ratio of rectangular jets with exit Mach number of 0.4 and 1. He concluded that sharp corners restrict the jet spread because of the actions of streamwise vortices. Low aspect ratio jets have high mass entrainment than the high aspect ratio jets. Various techniques of passive control of jets by introducing crosswire and tabs have been studied extensively by Rathakrishnan [13–15]. Stroher et al. [17] investigated the isothermal incompressible axisymmetric coaxial turbulent free jet using hot wire

***Corresponding author: S. Gopinath:** Bharath University, Chennai, India. E-mail: sundarsonic@yahoo.com
M. Sundararaj, S. Elangovan: Bharath University, Chennai, India
E. Rathakrishnan: Indian Institute of Technology Kanpur, Kanpur, India

anemometry. Decay of longitudinal and radial profiles of the velocity depends on the velocity ratio between the inner jet and coflow jet. Saiki et al. [18] states that the large-scale vortices were controlled by the excitation of outer shear layer using micro flap actuators. Regardless of the swirl intensity, large scale vortices shedding can be synchronized with flapping motion. Swirling coaxial jet control is effective for low swirl rate than the high swirl rate.

Non-circular jet with swirling co-flow has not received enough attention from the researchers and the present study is focused on the effect of swirling co-flow on the flow characteristics of such a flow field.

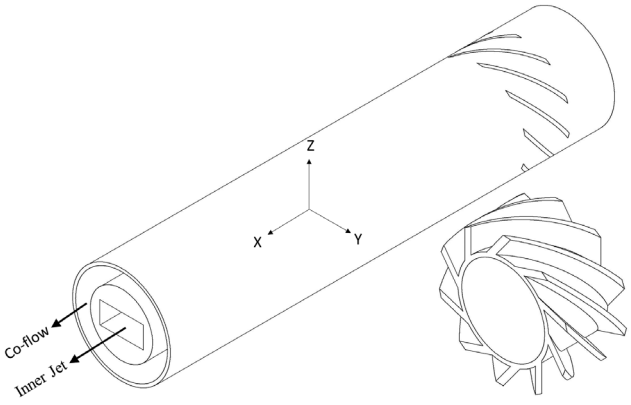

Fig. 2: Swirling co-flow setup, swirler design and axis orientation

2 Geometry

In this study three different inner jet nozzle exit shapes (circle, ellipse and rectangle) has been considered for three different co-flow conditions (no co-flow, straight co-flow and swirling co-flow). Dimensions of different inner jet nozzle and co-flow duct exit geometry were presented in Figure 1. All the inner jet configurations were designed such that its exit area ($A_e = 108$ mm^2) is constant and has an equivalent diameter of $D_e = 11.7$ mm.

For all three inner jet configurations co-flow is issued from an annular duct with an exit area of 410 mm^2. Inner diameter and outer diameter of the co-flow duct were 21 mm and 31 mm respectively. Mass flow ratio of the inner and co-flow jet is $m_{inner}/m_{co\text{-}flow} = 1.33$. Axis orientation and co-flow setup were shown in Figure 2. For all the inner jet and co-flow exit velocity was maintained as 250 m/s and 50 m/s respectively. Inner jet flow Reynolds number based on its equivalent diameter is Re = 200342.

Swirling co-flow is created by introducing a non-rotating swirler in the annular duct. Swirler has ten angular vanes which are 50° oblique to the jet axis. Distance between the co-flow exit and angular vanes were 150 mm this distance is adequate to create a fully developed swirling flow at the exit of the co-flow duct. Swirling co-flow is generally quantified by a dimensionless parameter called swirl number (S). It is defined as the ratio of the axial flux of angular momentum to the axial flux of axial momentum.

$$S = \frac{\int_{Ri}^{Ro} \rho u w_{tan} r^2 \, dr}{\int_{Ri}^{Ro} \rho u^2 r^2 \, dr} \tag{1}$$

Swirl number (S) calculated using Eq. (1) is equal to 0.92. Figure 3 shows the streamline pattern of the fully

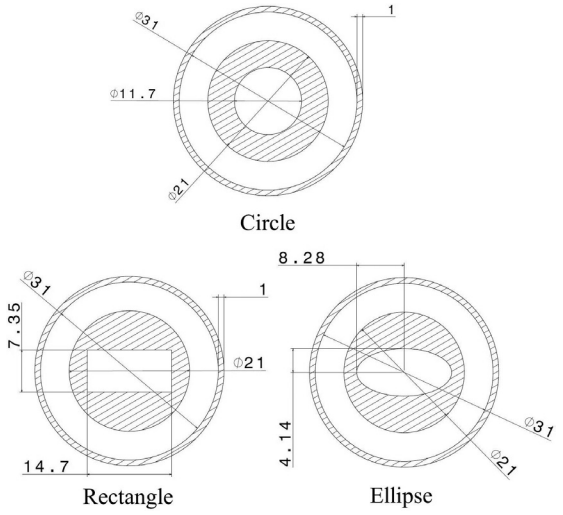

Fig. 1: Dimensions of different inner jet nozzle exit geometries

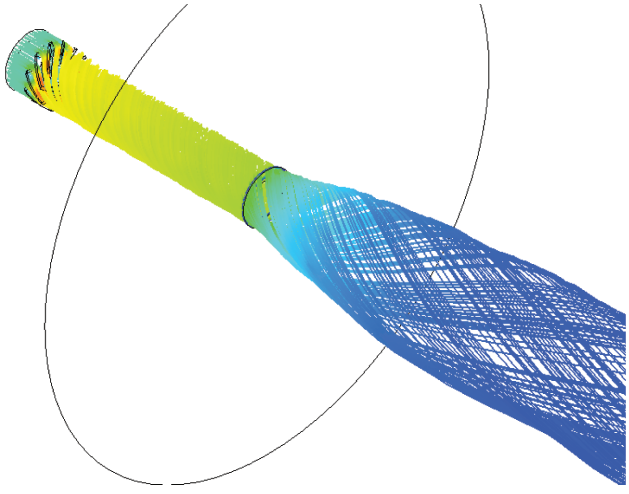

Fig. 3: Swirling co-flow created at the co-flow duct

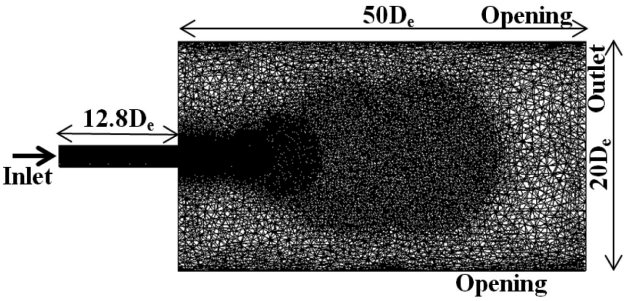

Fig. 4: Flow domain parameters based on exit diameter and mesh distribution

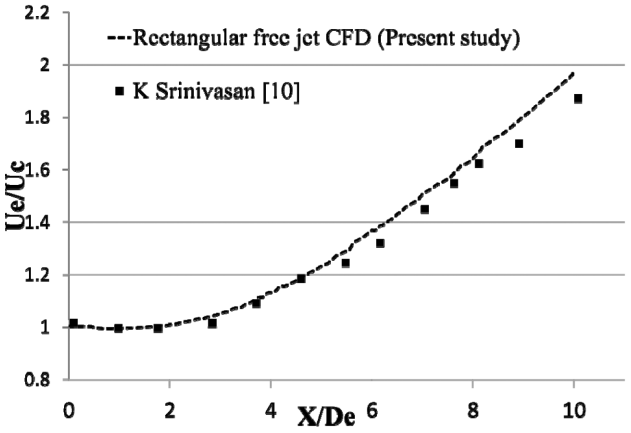

Fig. 5: Comparison between rectangular free jet CFD with Rectangular jet [10]

developed swirling coaxial jet issued from the circular annular co-flow duct.

3 Computational model

Computational domain used in this study is shown in Figure 4. The dimensions are based on the equivalent exit diameter $D_e = 11.7$ mm. Computational domain was discretized into a three dimensional grid consist of tetrahedral elements. To capture the jet core properties accurately, fine grid elements were used up to $2D_e$ in the radial direction from the jet center axis and axially up to $20D_e$ from the jet exit. Total number of elements and nodes used to construct the grid was 14×10^5 and 2.5×10^5 respectively. Reference pressure of 101325 Pa and ambient temperature of 288 K were used in the computational analysis.

To simulate the flow field a finite volume approach was used to solve the three dimensional Reynolds Averaged Navier Stokes (RANS) equation along with the Shear Stress Turbulence model (SST). To validate the selected boundary conditions and the domain parameters used in the present study, a comparison of inverse centerline velocity decay of computational results of rectangular free jet and experimentally measured rectangular free jet data of Srinivasan and Rathakrishnan [10] were plotted in Figure 5. It was found that they were in good agreement with each other.

A simplified notation for different jet configurations has been followed in the discussions here after is listed in Table 1. First letters C, E and R denote the three inner jet shapes Circle, Ellipse and Rectangle respectively. Second letters F, C and S denotes Free jet (no co-flow), Straight co-flow and Swirling co-flow respectively.

Table 1: Notations of different jet configurations

Geometry	Notations		
	Free jet	Straight co-flow	Swirling co-flow
Circle	CF	CC	CS
Ellipse	EF	EC	ES
Rectangle	RF	RC	RS

4 Results and discussions

4.1 Centerline velocity decay analysis

Variation of mean centerline velocity along the flow direction defines the overall characteristics of the jet flow field. This important phenomenon has been analyzed by plotting the normalized inverse centerline mean velocity against the non-dimensional axial distance of the different jet configurations considered for this study.

Centerline velocity decay of a jet has four different zones as shown in Figure 6. First zone is a core zone where the velocity of the jet is equal to the exit velocity. Zone two is a transition zone where the velocity starts to decay. Third zone is a profile similarity zone where the flow attains similar lateral velocity distribution profiles at different X/D_e locations. Fourth zone is a termination zone where, the jet decays in a rapid manner.

Malmstrom et al. [9] and Srinivasan and Rathakrishnan [10] used a simple decay expression (Eq. (2)) to fit the profile similarity zone of the velocity decay curves. Same equation was also used in the current study to fit the third zone ($X/D_e > 10$) of the velocity decay curve.

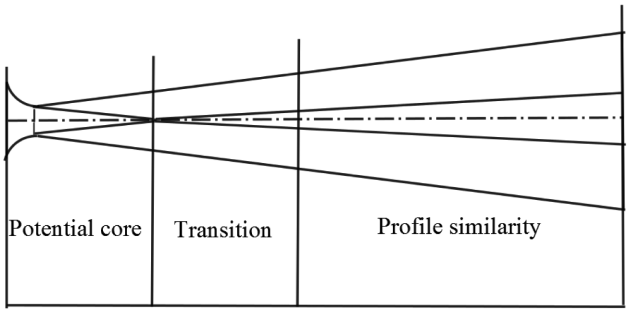

Fig. 6: Three different velocity decay zones of the jet

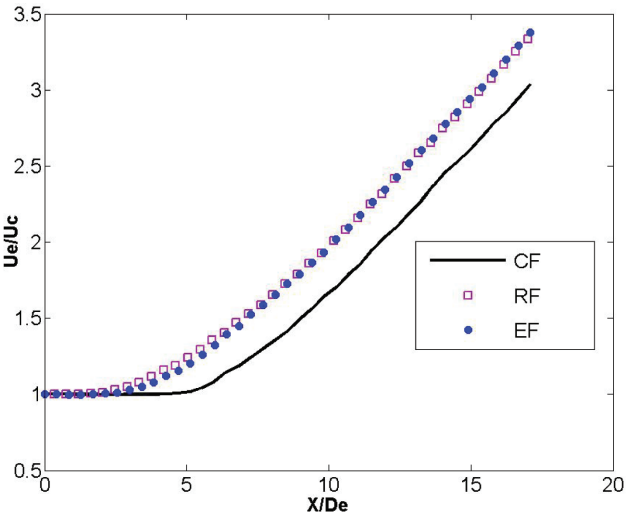

Fig. 7: Inverse velocity decay of different free jet configurations

$$\frac{U_e}{U_c} = K_u\left(\frac{X}{D_e} + C_u\right) \tag{2}$$

Figure 7 shows the centerline inverse velocity decay of different free jet configurations (circle, rectangle and ellipse). From the plot significant increase in velocity decay has been observed for the non-circular jet (RF and EF) configurations. For circular free jet (CF) jet the velocity decay starts at $X/D_e = 4.7$, this length of constant velocity region is known as the potential core length. Elliptical free jet (EF) jet has 53% shorter potential core length ($X/D_e = 2.2$) than the CF jet. RF jet has the shortest potential core length ($X/D_e = 1.9$) among the free jet configurations considered for this study, which is 60% shorter than CF jet and 14% shorter than EF jet. Potential core length for different jet configurations has been presented in Table 2. From the linear regression analysis of centerline inverse velocity decay rate of free jet configurations streamwise velocity decay rate (K_u) and kinematic virtual origin (C_u) has been obtained and listed in Table 3. Among the free jet configurations circular free jet has the highest value of K_u.

Table 2: Potential core length

Geometry	$X_{pc} * D_e$			Reduction of X_{pc} achieved by swirling co-flow (%)
	Free jet	Co-flow	Swirling co-flow	
Circle	4.7	4.9	4.7	5
Ellipse	2.2	2.4	2.0	17
Rectangle	1.9	1.9	1.6	16

Table 3: Values of K_u and C_u for different jet configurations

Geometry		Free jet	Co-flow	Swirling co-flow
K_u	Circle	0.1726	0.1487	0.1816
	Ellipse	0.1688	0.1293	0.403
	Rectangle	0.1623	0.1204	0.2838
C_u	Circle	0.0133	0.5185	−0.2996
	Ellipse	2.1694	3.7099	−0.2099
	Rectangle	2.7388	5.2317	0.9936

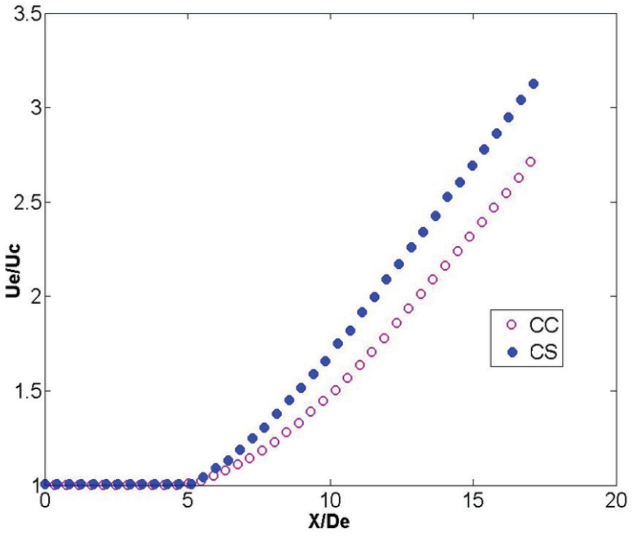

Fig. 8: Inverse velocity decay comparison between circular inner jet with straight co-flow (CC) and swirling co-flow (CS)

Centerline inverse velocity decay of circular inner jet with straight co-flow (CC) and circular inner jet with swirling co-flow (CS) has been plotted in Figure 8. From the plot it is evident that the swirling co-flow significantly increases the velocity decay of the circular jet. Potential core length of CC jet is higher than the circular free jet (Table 2). CS jet has 5% reduction in potential core length than the

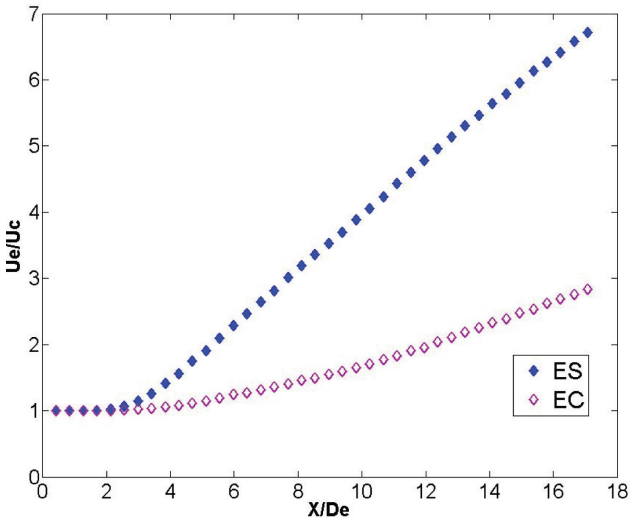

Fig. 9: Inverse velocity decay comparison between elliptical inner jet with straight co-flow (EC) and swirling co-flow (ES)

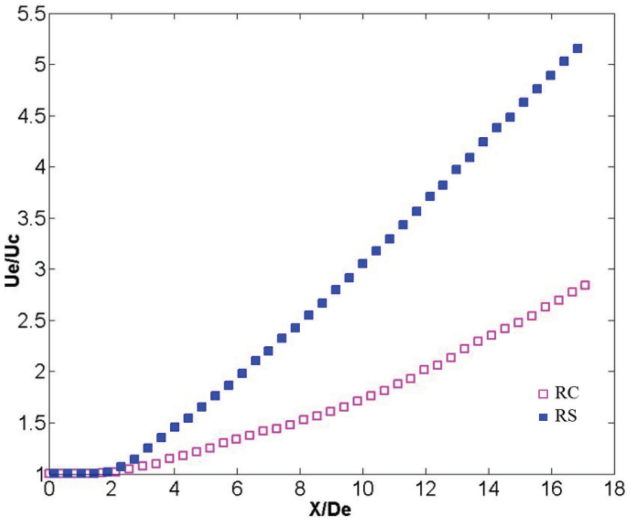

Fig. 10: Inverse velocity decay comparison between Rectangular inner jet with straight co-flow (RC) and swirling co-flow (RS)

CC jet but, it is equal to the potential core length of the circular free jet. From the linear regression analysis, CS jet has the highest streamwise velocity decay rate, which is 18% higher than the CC jet and 5% higher than the CF jet.

Comparison of centerline inverse velocity decay of elliptical inner jet with straight co-flow (EC) and elliptical inner jet with swirling co-flow (ES) has been shown in Figure 9. ES jet has the potential core length of $X/D_e = 2$ which is 17% shorter than the EC jet and 9% shorter than the EF jet configuration. As observed in circular jet with straight co-flow, in elliptical jet also introduction of straight co-flow significantly increase the potential core length. From the linear regression analysis, ES jet has the highest streamwise velocity decay rate of $K_u = 0.403$. Which is 68% higher than the K_u value of EC and 58% higher than the EF jet.

Figure 10 shows the comparison of centerline inverse velocity decay of rectangular inner jet with straight co-flow (RC) and rectangular inner jet with swirling co-flow (RS). It is observed that the potential core length of the RC jet is equal to RF jet. But RS jet has 16% less potential core length than the RC jet configuration. As observed in the case of circular and elliptical inner jet cases, in rectangular jet also, introduction of straight co-flow reduces the streamwise velocity decay rate (K_u). K_u value of RS jet is 58% higher than the RC jet and 43% higher than the RF jet configurations.

In general, issuing straight co-flow from the circular annular duct over the inner jet flow increases the potential core length of circular and elliptical inner jet by 4% and 8% respectively. But it made no changes in potential core length of rectangular inner jet configuration. Straight co-flow, also reduces the streamwise velocity decay rate of circular, elliptical and rectangular inner jets by 16%, 30% and 35% respectively. Introduction of swirling co-flow reduces the relative velocity between the jet and surrounding air so, it acts as a boundary to the inner jet and prevents the jet from mixing with the surrounding air. But swirling co-flow forces the inner jet to rotate around its axis, and reduces the potential core length. Thus, it increases the streamwise velocity decay rate of the inner jet.

Elliptic inner jet with swirling co-flow has the highest value of K_u among the jet configurations considered for the current study. Thus, it may be stated that the swirling co-flow has higher influence on elliptical inner jet than the circular and rectangular inner jet. Circular jet has comparatively less influence of swirling co-flow than the other two inner jet configurations. K_u value of RF jet is 0.1623 which is in agreement with the previous literature values. Quinn [11] obtained a value of $K_u = 0.155$, and Srinivasan and Rathakrishnan [10] obtained a value of $K_u = 0.1786$. Value of K_u obtained for RF jet in this study has fallen between these two literature values. This difference is may be due to that the flow conditions considered for the studies may have little differences.

4.2 Lateral velocity distribution

Lateral velocity distribution along Y and Z axis for different jet configurations has been shown in Figures 11 and 12 respectively. Since the lateral velocity distribution plots at $X/D_e = 0$ and $X/D_e = 1$ were located at the potential core region, not much difference has been observed between

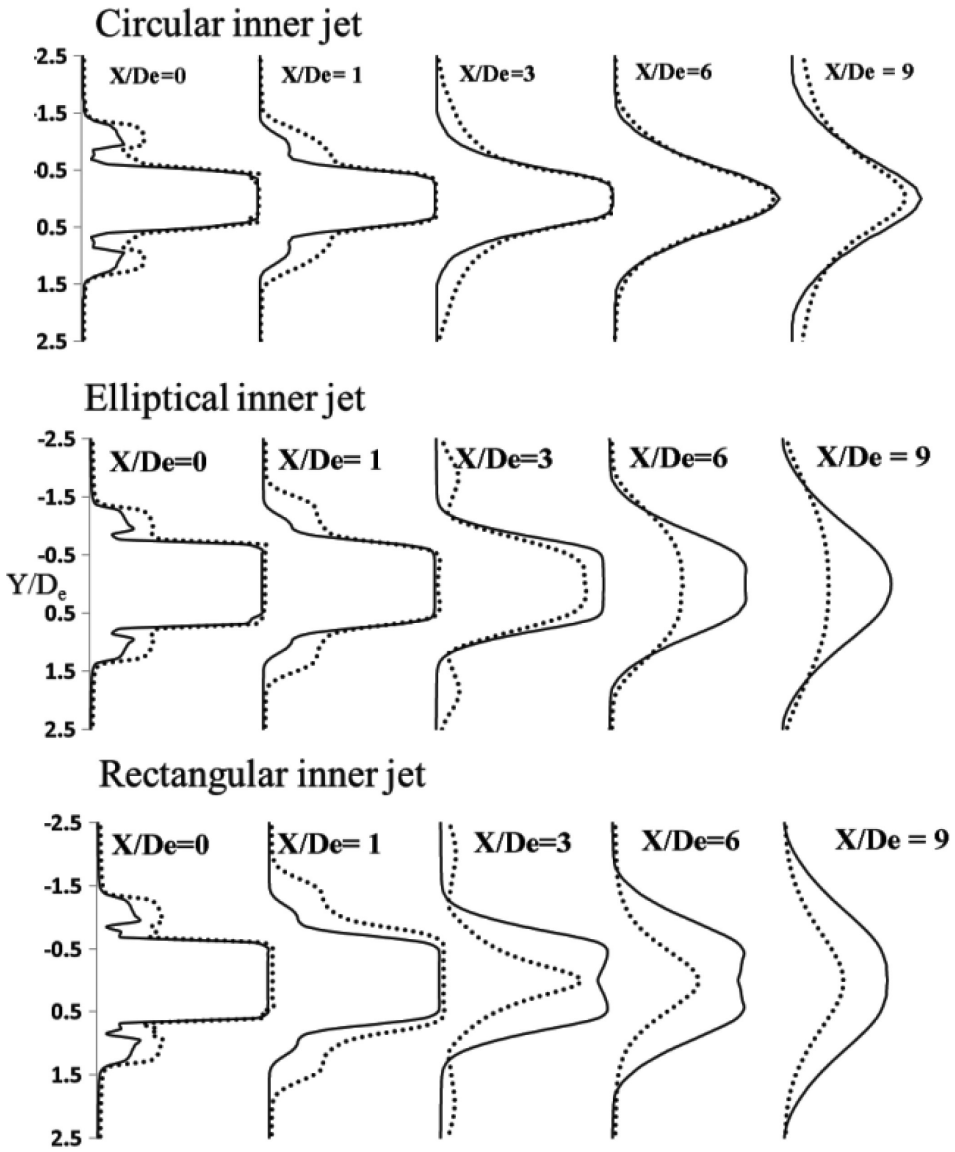

Fig. 11: Velocity distribution in XY plane at various X/D locations (X axis – U/U_e and Y axis – Y/D_e, ____ – jet with straight co-flow, ... – jet with swirling co-flow)

the inner jer with straight and swirling coflow configurations. But at $X/D_e = 3$ rectangular and elliptical with swirling coflow has less maximum velocity at $Y/De = 0$ and $Z/De = 0$, this difference in maximum velocity occours due to inner jet (rectangle and ellipse) with swirling coflow starts to decay faster than that of straight coflow. At $X/D_e = 3$, from the lateral velocity distribution plot (Y and Z) of elliptical and rectanglar inner jet configuration, it can be observed that the straight coflow confuguration has a flat maximum velocity region when compared to the maximum velocity region of swirling coflow. This difference is due to that the swirling coflow reduces the maximum velocity region width of inner jet. At $X/D_e = 3$ of Y axis velocity distribution of rectangular jet with straight coflow, a small drop in velocity is observed at $Y/D_e = 0$. This drop occours may be due to the action of streamwise vortex in the rectangular inner jet flow field. But this dip is not observed in the case of rectangular inner jet with swirling coflow.

From the lateral velocity distribution of Figures 11 and 12 at $X/D_e = 9$ sgnificant difference is obsereved between the straight and swirling coflow conditions. Local maximum velocity of the jet with swirling coflow was smaller than the inner jet with straight coflow. Jet spread also more for jet with swirling coflow than the other configuration. All jet configurations attains self similarity in lateral velocity distribution at $X/D_e = 9$. In Figure 12 lateral velocity distribution plot of rectangle and elliptical jet

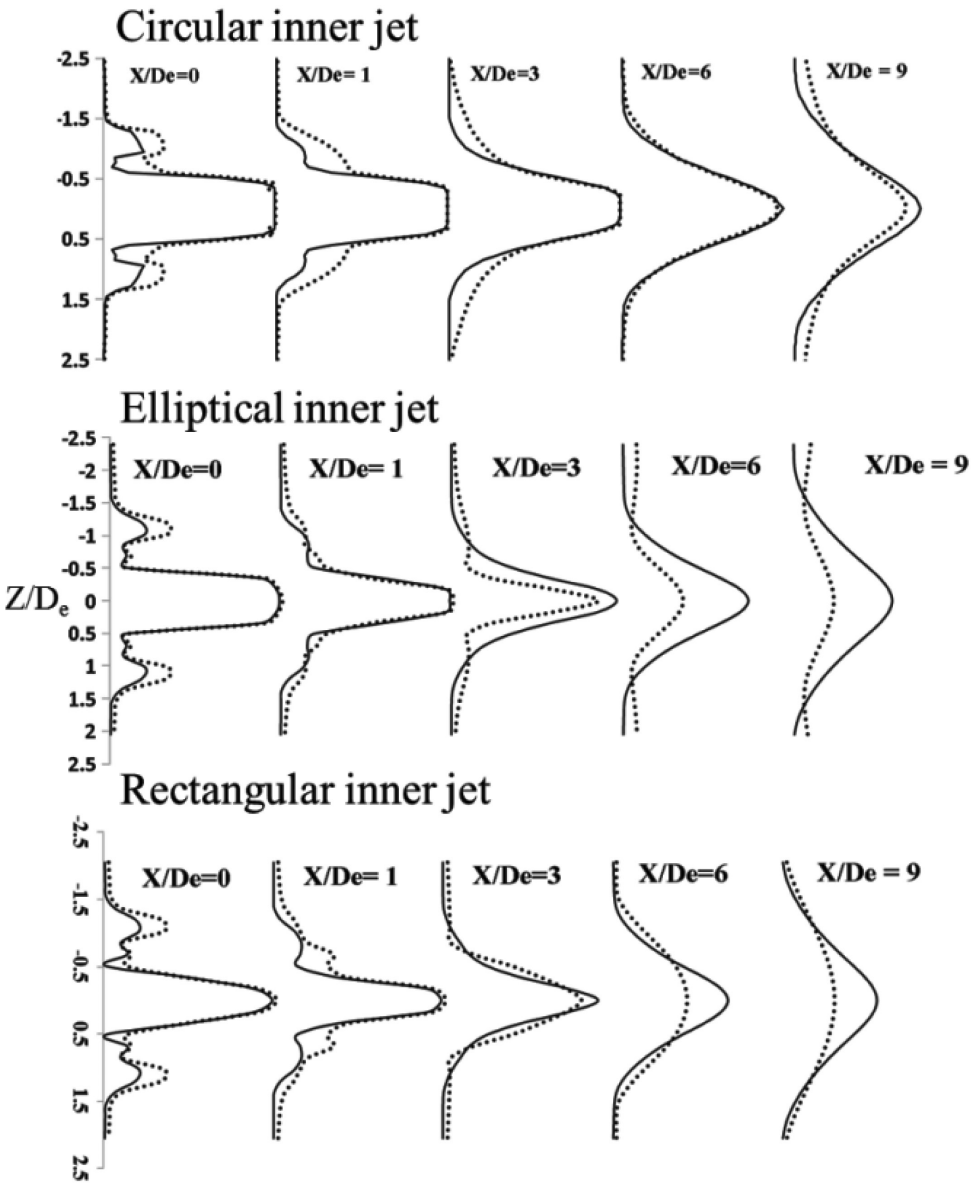

Fig. 12: Velocity distribution in XZ plane at various X/D locations (____ – jet with straight co-flow, ... – jet with swirling co-flow)

width of the peak reduces upto $X/D_e = 3$ and increases after $X/D_e = 3$. This tendency was may be due to the axis switching of rectangular and elliptical jets.

4.3 Mass entrainment

Normalized mass entrainment of inner jet (circle, ellipse and rectangle) with straight and swirling co-flow along the streamwise direction has been plotted in Figure 13. m_0/m is a ratio of mass flow rate through a plane at $X/D_e = 0$ to the mass flow rate through a plane at corresponding X/D_e locations. From the plot it is evident that the entrainment is more for the swirling co-flow than straight co-flow. Upto $X/D_e = 2$ there is no significant difference between the mass entrainment of different jet configurations. Streamwise mass entrainment rate (K_m) were calculated by linear regression analysis of the entrainment curves plotted in Figure 13 which has been listed in Table 4. In Figure 13 mass entrainment at locations $X/D_e > 4$ is considered for calculating streamwise mass entrainment rate (K_m).

Among the three inner jet with straight co-flow configurations elliptical jet has the highest mass entrainment rate of $K_m = 0.0664$, which is 16% and 2% higher than the K_m value of circular jet and rectangular jet with straight

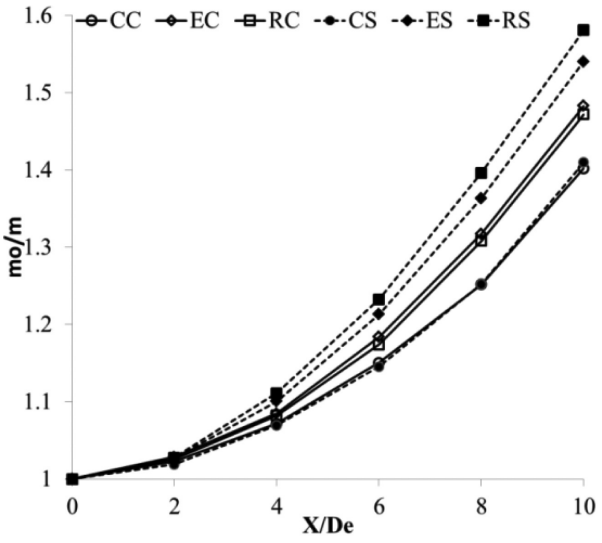

Fig. 13: Mass entrainment of different jet configurations at various X/D locations

Table 4: Streamwise mass entrainment rate

Geometry	K_m	
	Straight co-flow	**Swirling co-flow**
Circle	0.0547	0.0564
Ellipse	0.0664	0.0735
Rectangle	0.0652	0.0787

co-flow. But in the case of swirling co-flow, rectangular jet has 28% and 7% higher mass entrainment rate (K_m) than circular and elliptical shape inner jet.

Large and small scale mixing are the important factors affecting the mass entrainment. Small scale mixing of the jet was largely influenced by the streamwise corner vortices which are created due to the azimuthal variation in the nozzle exit geometry. Streamwise corner vortices developed in the inner jet flow field has been shown in Figure 14 in the form of tangential velocity vector plot at cross sectional plane located at X/De = 1. Sample points considered to plot the velocity vector plot were equally spaced on the considered YZ plane and the base size of the arrow also maintained same for all the plots. Length of the arrow is proportional to the magnitude of the velocity at local corresponding points. From the vector plot it can be observed that the rotation of vortices was such that the every vortex rotates in the opposite direction to the adjacent vortices, except the diagonal vortex.

EC and RC jet have four streamwise vortices. The entrainment of the surrounding fluid takes place exactly in same pattern for these two jet configurations. But the magnitude of velocity of the entrainment fluid for RC jet was more when compared with EC jet. Corner vortices of RC jet are closer to the minor axis than the corner vortices of EC jet. For the EC and RC jet the fluid from the surroundings entrains more through the surface parallel to the major axis plane than surface parallel to the minor axis plane. Due to the action of streamwise corner vortices at the corners the fluid entrainment is very less when compared with other regions. So this may be the reason for that the jet spread is restricted in the direction of corners as stated by Srinivasan and Rathakrishnan [10].

Circular jet with straight co-flow (CC) has no streamwise vortices as observed in Figure 14. But when swirling co-flow was introduced four stream wise vortices has been created at the inner jet flow field. This was due to that the inner jet is forced to swirl around its axis. This causes the inner jet flow near the interface surface of inner jet and swirling co-flow jet to rotate in the direction of the swirling co-flow. But, this effect is less in the core of the inner jet when compared with the flow field near the interface. This difference in velocity magnitude at the different regions of inner jet flow induces the formation of streamwise vortices in CS configuration.

Introduction of swirling co-flow reduces the number of streamwise vortices in the rectangular and elliptical inner jet flow field. And also it displaces the location of the vortices. For swirling co-flow jets it was observed that the size of the streamwise vortices also increased when compared with the straight co-flow case. Thus, it may be said that swirling co-flow interacts more with the surrounding fluid than the straight co-flow hence it increases the entrainment of the surrounding air with the jet.

4.4 Jet spread

Jet spread or jet growth is characterised by the half jet width. Half jet width of a jet is defined as the distance between the jet centerline and where the local velocity is equal to the half of the centerline mean velocity. Half width of different inner jet with straight coflow has been plotted in Figure 15. Location of axis switching of elliptical inner jet with straight coflow (EC) can be observed as $3.1D_e$, which is in very good agreement with the literature value of $3D_e$ of Miller et al. [6]. For RC, axis switching occours at $2D_e$ but for Srinivasan and Rathakrishnan [10] the value is $2.5D_e$. Half width of different inner jet with swirling coflow was plotted in Figure 16. From the plot it was observed that after $X/D_e = 7$ the Y/D_e and Z/D_e values varies linearly. The half widths ($X/D_e > 7$) of different jet configurations has been fitted in to a linear Eq. (3) to

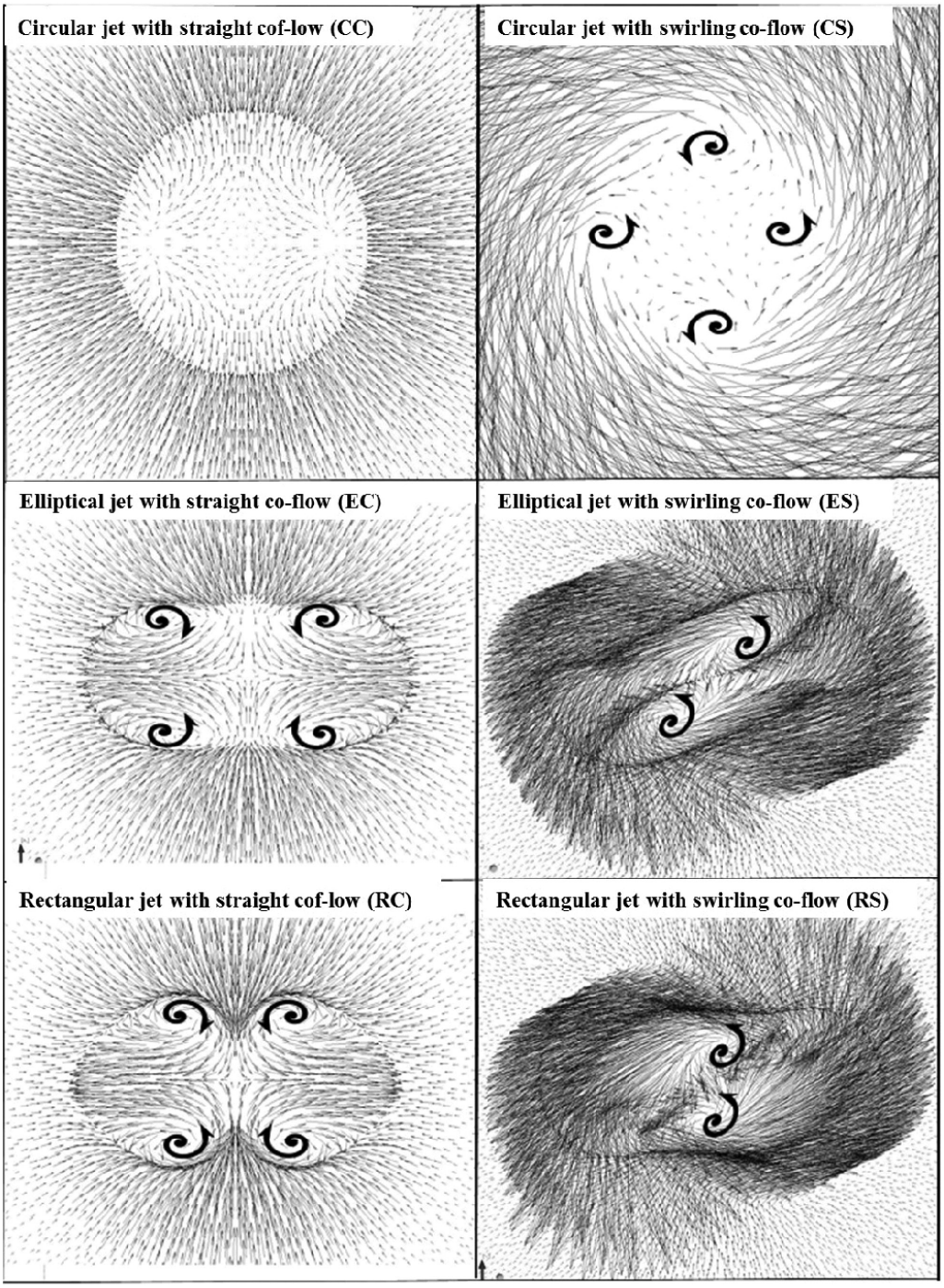

Fig. 14: Streamwise corner vortex pattern for different jet configurations ($X/D_e = 1$)

calculate the value of K_s and C_s.

$$\frac{Y_{0.5}}{D_e} = K_s\left(\frac{X}{D_e} + C_s\right) \tag{3}$$

Calculated values of K_s and C_s along Y and Z axis were tabulated in Tables 5 and 6. From Tables 5 and 6, for all the inner jet configurations introduction of swirling coflow increases the far-field spreading rate (K_s) when compared with straight coflow along both the axis (Y and Z). Swirling coflow increases the spreading rate of circular, elliptical and rectangular jet by 10, 12 and 16 percentage along Y axis (10, 12 and 5 percentage along Z axis) respectively when compared with straight coflow. Circular jet with

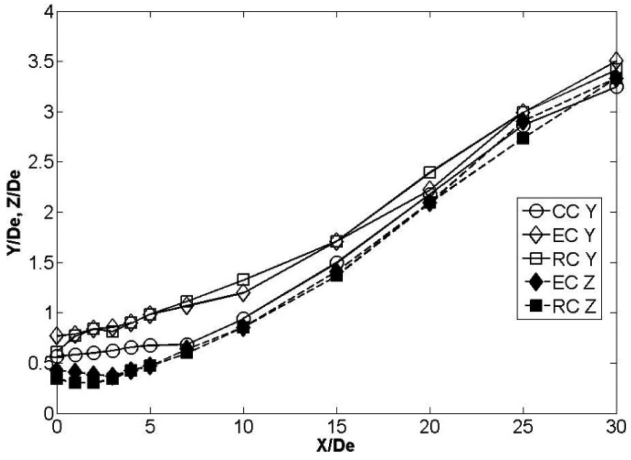

Fig. 15: Half jet width of different inner jet with straight coflow

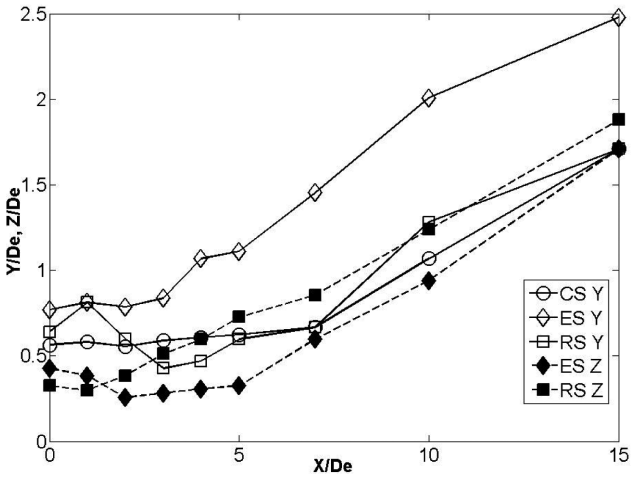

Fig. 16: Half velocity width of different inner jet with swirling coflow

Table 5: Values of K_s and C_s for different jet configurations at Y axis

Geometry	K_s		C_s	
	Co-flow	Swirling co-flow	Co-flow	Swirling co-flow
Circle	0.1171	0.1301	−1.5858	−1.997
Ellipse	0.1103	0.1247	1.3499	5.2101
Rectangle	0.1048	0.1258	2.7586	−0.9706

straight coflow (CC) has the highest spreading rate along Y axis when compared with other jets (EC and RC) configurations and elliptical jet with straight coflow (EC) has the highest spreading rate along Z axis.

Table 6: Values of K_s and C_s for different jet configurations at Z axis

Geometry	K_s		C_s	
	Co-flow	Swirling co-flow	Co-flow	Swirling co-flow
Circle	0.1171	0.1301	−1.5858	−1.997
Ellipse	0.1235	0.1404	−2.6712	−2.9566
Rectangle	0.1219	0.1282	−2.8171	−0.3331

5 Conclusions

Centerline velocity decay, mass entrainment, jet spread and corner vortex behavior of subsonic compressible non-circular jet (circle, ellipse and rectangle) with straight and swirling co-flow have been studied in detail. Among the free jet configurations rectangular free jet has the potential core length of $1.9D_e$ which is 60% shorter than circular free jet and 14% shorter than elliptical free jet. But circular free jet has the highest value of streamwise velocity decay rate. Thus, from the jet configurations considered for this study, it may be stated that the jet with shortest potential core length has lowest streamwise velocity decay rate in profile similarity region. Introduction of straight co-flow over the inner jet configuration results in increase of potential core length and decrease of streamwise velocity decay rate. But, introduction of swirling co-flow over the inner jet results in the decrease of potential core length, increase of streamwise velocity decay rate, increase of the entrainment of surrounding fluid, and increase of jet spread, compared to the straight co-flow configuration. Among the inner jet with swirling co-flow configurations maximum reduction of potential core length (17%) and streamwise velocity decay rate (68%) is achieved in elliptical inner jet when compared with straight co-flow configuration. Mass entrainment and jet spread also significantly increased by swirling co-flow for the elliptical jet configuration. Thus, it may be stated that the effect of swirling co-flow is higher on the elliptical inner jet than the other inner jet configurations.

Nomenclature

ρ	density
A_e	exit area (mm^2)
C_s	geometric virtual origin
C_u	kinematic virtual origin of the jet
D_e	equivalent exit diameter (mm)
K_s	far field spreading rate

K_u	streamwise velocity decay rate along the centerline
m_{coflow}	coflow mass flow rate (kg/s)
m_{inner}	inner jet mass flow rate (kg/s)
r	radial co-ordinate (m)
R_o, R_i	outer and inner diameter of the annular duct (m)
Re	Reynolds number
S	swirl number
u, w_{tan}	axial and swirling component of the velocity (m/s)
U_c	centerline velocity along streamwise direction (m/s)
U_e	exit velocity of inner jet (m/s)
X_{pc}	potential core length
$Y_{0.5}$	half velocity width in Y-direction
$Z_{0.5}$	half velocity width in Z-direction

Acknowledgments: The authors greatly acknowledge the Center for Aerospace Research, Madras Institute of Technology (MIT), Anna University, Chennai, India for providing computational facilities and Mr. G. Nagamanikandan, Postgraduate student of MIT, Chennai for assisting in computation.

References

[1] Hussein H. J., Capp S. P. and George W. H., "Velocity Measurements in a High-Reynolds-Number, Momentum-Conserving, Axisymmetric, Turbulent Jet", Journal of Fluid Mechanics, Vol. 258, 1994, pp. 31–75.

[2] Gutmark J. and Grinstein F. F., "Flow Control with Noncircular Jets", Annual Review of Fluid Mechanics, Vol. 31, No. 1, 1999, pp. 239–272.

[3] Bogey C. and Bailly C., "A Study of the Influence of the Reynolds Number on Jet Self-similarity Using Large-Eddy Simulation", Proceedings of Seventh International ERCOFTAC, 2008.

[4] Bogey C. and Bailly C., "Effects of Inflow Conditions and Forcing on Subsonic Jet Flows and Noise", AIAA Journal, Vol. 43, No. 5, 2005, pp. 1000–1007.

[5] Zaman K. B. M. Q. and Wang F. Y., "Noise, Turbulence and Thrust of Subsonic Free Jets from Lobed Nozzles", AIAA-2002-0569.

[6] Miller R. S., Mandia C. K. and Givi P., "Numerical Simulation of Non-Circular Jets", Computers & Fluids, Vol. 24, 1995, pp. 1–25.

[7] Ocer N. E., Tasar G., Uzol O. and Ozgen S., "Flow Structure and Turbulence in Near Fields of Circular and Noncircular Jets", Flight Physics, Vol. 3, 2012, pp. 41–52.

[8] Menter F. R., "Performance of Popular Turbulence Models for Attached and Separated Adverse Pressure Gradient Flows", AIAA Journal, Vol. 30, No. 8, 1992, pp. 2066–2072.

[9] Malmstrom T. G., Kirkpatrick A. T., Christensen B. and Knappmiller K. D., "Centerline Velocity Decay Measurements in Low-velocity Axisymmetric Jets", Journal of Fluid Mechanics, Vol. 246, 1997, pp. 363–377.

[10] Srinivasan K. and Rathakrishnan E., "Morphology of Subsonic Rectangular Slot Jets", Proc. IMechE, Vol. 222, Part G: J. Aerospace Engineering, Vol. 222, No. 4, 2008, pp. 449–461.

[11] Quinn W. R., "Turbulent Free Jet Flows Issuing from Sharp-Edged Rectangular Slots:The Influence of Slot Aspect Ratio", Experimental Thermal and Fluid Science, 1992, pp. 203–215.

[12] Wilcox D. C., "Multiscale model for turbulent flows", AIAA Journal, Vol. 26, No. 11, 1988, pp. 1311–1320.

[13] Phanindra C. and Rathakrishnan E., "Corrugated Tabs for Supersonic Jet Control", AIAA Journal, Vol. 48, No. 2, 2010, pp. 453–465.

[14] Thanigaiarasu S., Elangovan S. and Rathakrishnan E., "Effect of Arc-In Tab on Mixing Characteristics of High Speed Jets," 10th Asian Symposium on Visualization, Part 1, 2010.

[15] Lovaraju P. and Rathakrishnan E., "Shifted Cross-Wire for Jet Flow Control", International Review of Aerospace Engineering (IREASE), Vol. 1, No. 1, 2008, pp. 61–68.

[16] Liang H. Z. and Maxworthy T., "An Experimental Investigation of Swirling Jets", J. Fluid Mechanics, Vol. 525, 2005, pp. 115–159.

[17] Ströher G. R., Martins C. A. and De Andrade C. R., "Numerical and Experimental Study of a Free Incompressible Isothermal Turbulent Coaxial Jet", Thermal Engineering, Vol. 9, No. 1, 2010, pp. 98–107.

[18] Saiki Y., Suzuki Y. and Kasagi N., "Active Control of Swirling Coaxial Jet Mixing with Manipulation of Large-scale Vortical Structures", Flow, Turbulence and Combustion, Vol. 9, No. 3, 2004, pp. 399–418.